scientific reports

Check for updates

OPEN

Effectiveness and mechanism of cisplatin combined with PDT on human lung adenocarcinoma A549 cells transplanted tumor in nude mice

Tong Li, Xiao-hui Yang, Ming-ju Shao, Yu-xia Dong, Lin-yu Li & Cun-zhi Lin✉

This study aims to investigate the effect and mechanism of photodynamic therapy (PDT) combined with cisplatin on human lung adenocarcinoma A549 cells transplanted tumors in nude mice, and to provide a theoretical basis for clinical PDT. Construction of a nude mouse lung cancer transplantation tumor model using the human lung adenocarcinoma A549 cell line, and the mice were randomly divided into four groups: the control group, the cisplatin alone group, the PDT alone group, and the cisplatin combined PDT group. The apoptosis of tumor cells in the four groups was observed and compared by the TUNEL method, and the mRNA expression levels of apoptosis-related genes Bax, caspase-3 and Survivin, as well as the expression levels of the corresponding proteins, were detected by the real-time fluorescence quantitative polymerase chain reaction (RT-qPCR) and the protein immunoblotting technique (Western blot) respectively. The results showed that photodynamic force combined with cisplatin was effective in inhibiting tumor growth, and its effect was superior to that of cisplatin or PDT alone. This may be related to the promotion of apoptosis, specifically through the up-regulation of Bax and caspase-3, and the down-regulation of Survivin gene expression, thus inhibiting cell proliferation.

Keywords Photodynamic therapy, Lung adenocarcinoma, Animal model, Angiogenesis, Apoptosis

Global lung cancer cases and mortality rates are increasing. GLOBOCAN's 2018 data estimated 2.09 million new cases (11.6% of all cancer cases) and 1.76 million deaths (18.4% of all cancer deaths)[1,2]. Compared to 2012 reports (1.8 million new cases and 1.6 million deaths), this trend has grown significantly[3]. The main cause of cancer is long-term smoking, and radon, asbestos, silica, nickel and AIDS also contribute to the progression of lung cancer[4]. However, only about 15% of patients are diagnosed with cancer that is confined to the early stages. More patients are in advanced stages, suffering from dyspnea, coughing up blood, obstructive pneumonia, respiratory failure, and other painful conditions[5]. Therefore, the search for a targeted and efficient treatment has become a focus of research.

Photodynamic Therapy (PDT) has garnered interest as a local treatment due to its ability to exploit the differential affinity of photosensitizers between tumor and normal tissues, leading to higher photosensitizer concentrations within tumor tissues[4]. Photosensitized tissues, upon laser irradiation, generate singlet oxygen and free radicals that impact tumor cell growth, ultimately leading to cell death[6]. PDT minimizes damage to normal tissues due to differential photosensitizer concentrations in tumors versus normal tissues. Even in case of mild tissue damage, rapid recovery is typically observed[7,8]. Additionally, PDT stimulates immune cells initiating a specific immune response against tumor cells upon infiltration into tumor tissues[5,9–11]. Currently, PDT is widely used in the treatment of cancer, such as skin cancer. However, its effectiveness is limited in treating deep lesions and distant metastases due to the laser's inability to penetrate deep tissues[12] and the potential for allergic reactions and toxicity of photosensitizers limit the use of PDT in tumor therapy[13,14]. Efforts have been made to enhance PDT efficacy by combining it with various treatments, including chemotherapy using cisplatin. Cisplatin is a common cancer treatment that binds to DNA, inhibiting cancer cell division, preventing DNA replication, and ultimately inducing cancer cell death[15–17]. However, cisplatin's long-term use decreases

Department of Respiratory and Critical Care Medicine, The Affiliated Hospital of Qingdao University, Qingdao 266003, China. ✉email: lindoc@126.com

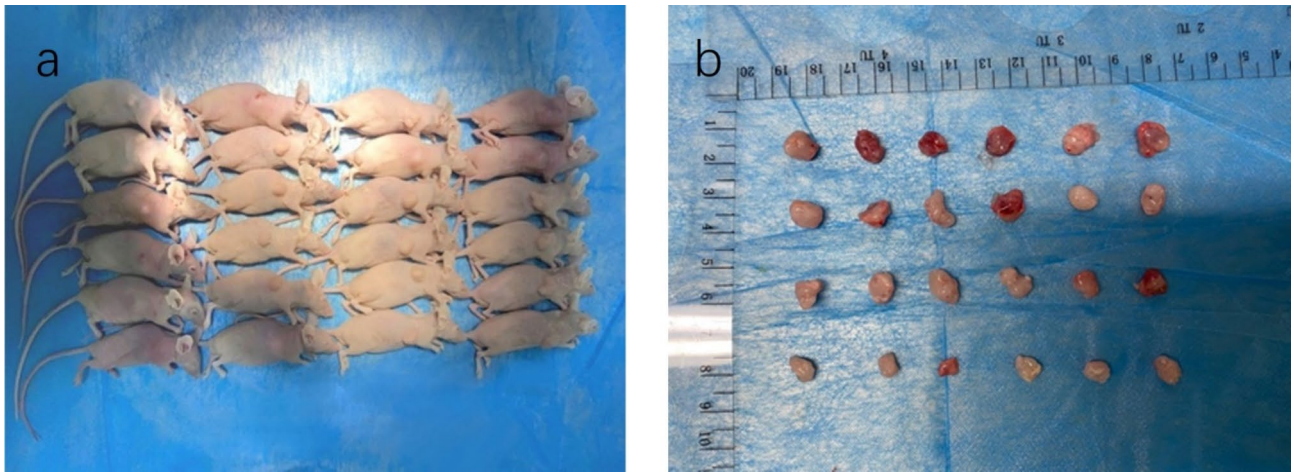

Fig. 1. Construction of an animal model of lung adenocarcinoma A549. (**a**) Nude mice were executed by dislocation method 12 days after the last treatment, and all nude mice were seen to have tough subcutaneous nodules. From left to right: control group, cisplatin alone group, PDT alone group, cisplatin combined with PDT group. (**b**) Blunt separation of the subcutaneous mass with scissors reveals grayish-red, hemorrhagic tumor tissue that is adherent to the surrounding tissue. From top to bottom: control group, cisplatin alone group, PDT alone group, cisplatin combined with PDT group.

Days	Control group	Cisplatin alone group	PDT alone group	Cisplatin combined with PDT group
0	0.00	0.00	0.00	0.00
7	51.27 ± 4.69	50.07 ± 4.55	49.25 ± 5.11	49.78 ± 4.43
10	63.85 ± 7.11	63.66 ± 6.01	65.52 ± 6.53	58.66 ± 7.24
13	77.87 ± 8.98	78.75 ± 10.54	77.73 ± 11.04	71.12 ± 9.89
16	98.52 ± 12.56	95.33 ± 11.67	91.64 ± 13.28	85.57 ± 11.46
19	149.98 ± 17.34	130.84 ± 15.98	120.25 ± 18.93	98.61 ± 16.52
22	219.71 ± 45.57	183.75 ± 59.76	168.33 ± 56.87	119.27 ± 50.34
25	352.53 ± 69.62	300.82 ± 91.15	280.77 ± 80.36	190.51 ± 70.28

Table 1. Changes in tumor volume growth in each group (mm^3, $\bar{x} \pm s$ n = 6).

tumor responsiveness and can damage the liver, kidneys, and bone marrow hematopoiesis. Recent studies have demonstrated the potential benefits of combining PDT with cisplatin chemotherapy. This study established a nude mouse xenograft model of lung adenocarcinoma and investigated the therapeutic effects and mechanisms of PDT, using HPD-mediated 630-nm laser combined with cisplatin chemotherapy. Photosensitizers were locally injected, and multiple low-dose laser irradiation was applied to provide a theoretical basis for the clinical application of PDT combined with chemotherapy in treating lung cancer.

Results

Construction of an animal model of lung adenocarcinoma A549

About 5–7 days after inoculation, subcutaneous tough nodules of 5–7 mm appeared at each inoculation site in nude mice, which were round or oval in shape, suggesting successful establishment of the model, followed by gradual enlargement of the tumors. In this study, the hematoporphyrin was locally injected in three points around the transplanted tumor in nude mice, ensuring direct delivery to the target site. Although cisplatin is administered intraperitoneally, its well-known pharmacokinetic properties ensure that it is distributed to tumor tissue where it exerts its cytotoxic effects[18]. Until 12 days after the last treatment to execute all nude mice. On the sixth day after the end of treatment, the tumor volume of the nude mice in the 3 treatment groups grew slowly and the average volume began to be smaller than that of the control group, compared with the blank control group, and the effect of the cisplatin combined with PDT group was particularly obvious(Fig. 1). Table 1 shows the changes in tumor volume growth in each group.

Microscopically, Fig. 2 shows the 4 groups of lung cancer cells were seen to be numerous and closely arranged, with large, deeply stained nuclei and many nuclear schizophrenic images. The interstitium was loose and stained pink, which showed that the lung adenocarcinoma A549 animal model was successfully established.

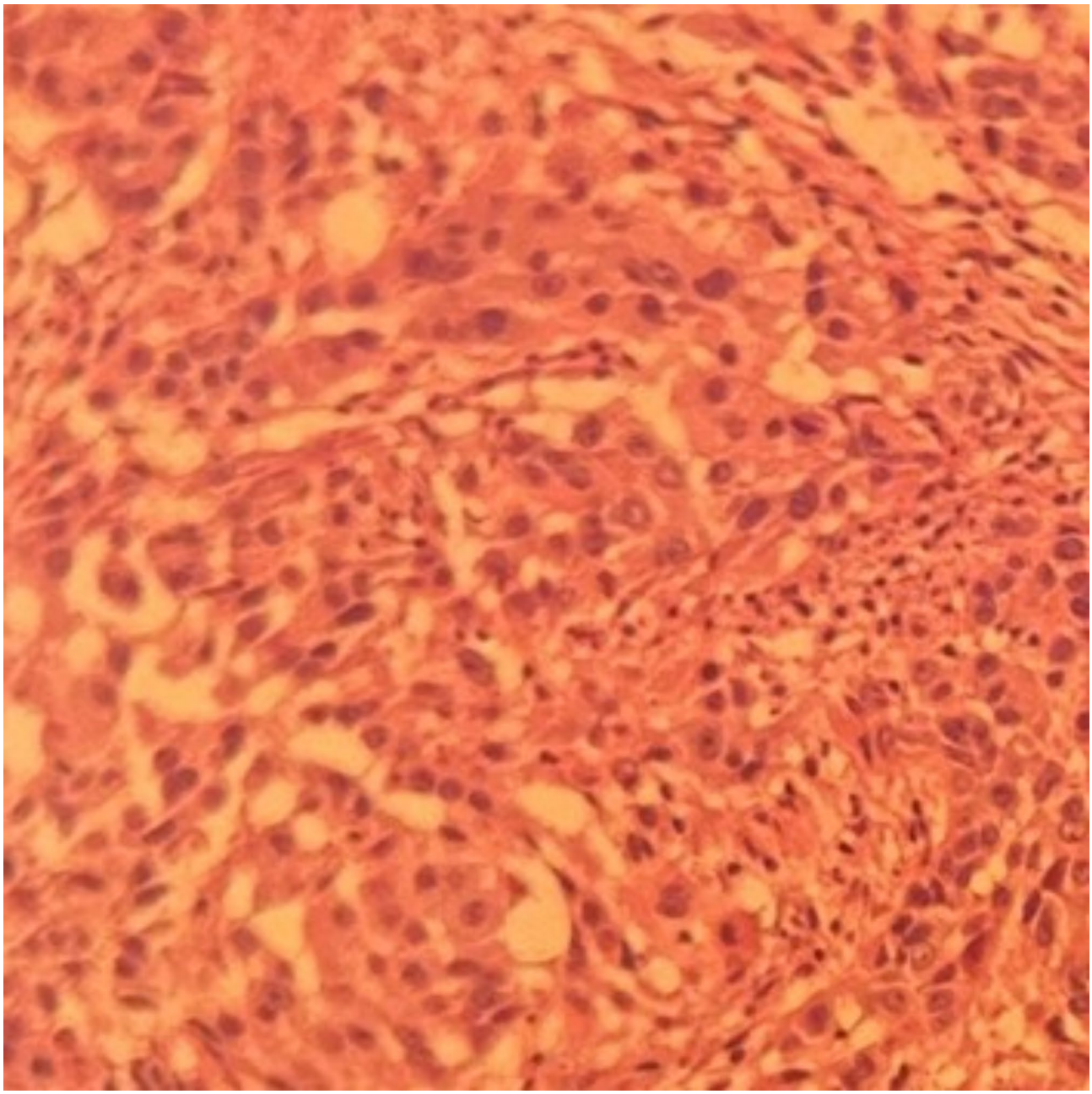

Fig. 2. Under HE staining, the tumor cells became spindle-shaped with large and deeply stained nuclei, suggesting that the lung adenocarcinoma A549 transplantation tumor model was successfully established.

TUNEL staining method to detect apoptosis

Apoptotic cells were seen in the tissue sections of transplanted tumors in all groups of nude mice. Figure 3 shows that apoptotic cells were scattered among the tumor cells with reduced cytoplasm; brownish-yellow granular material was seen in the nucleus of the cells, which manifested the phenomenon of nuclear fragmentation, nuclear consolidation or nuclear lysis. Compared with the other 3 groups, apoptosis-positive cells increased significantly in the combination group, and the apoptosis phenomenon was most obvious. 5 high magnification fields of view with the highest number of positive cells were selected from the TUNEL sections of each group, and the apoptotic index, i.e., the percentage of apoptotic cells to all cells in the field of view, was calculated. The apoptotic index was 1.5%, 4.6%, 5.6% and 9.5% in the control group, the cisplatin alone group, the PDT alone and the combination group, respectively. The latter 3 groups were significantly higher than the control group ($P < 0.05$), and the difference was statistically significant.

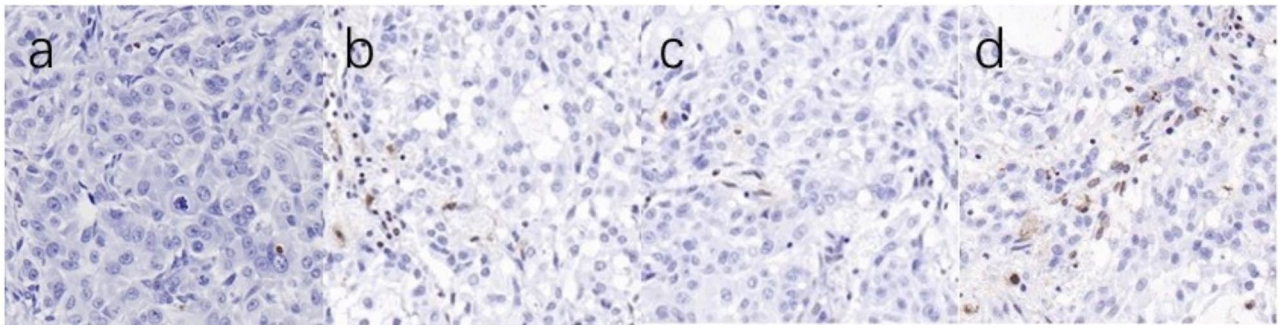

Fig. 3. Brownish-yellow granules were seen in the nuclei of apoptotic cells after TUNEL staining. (**a**) Control group, (**b**) Cisplatin alone group, (**c**) PDT alone group, (**d**) Cisplatin combined with PDT group.

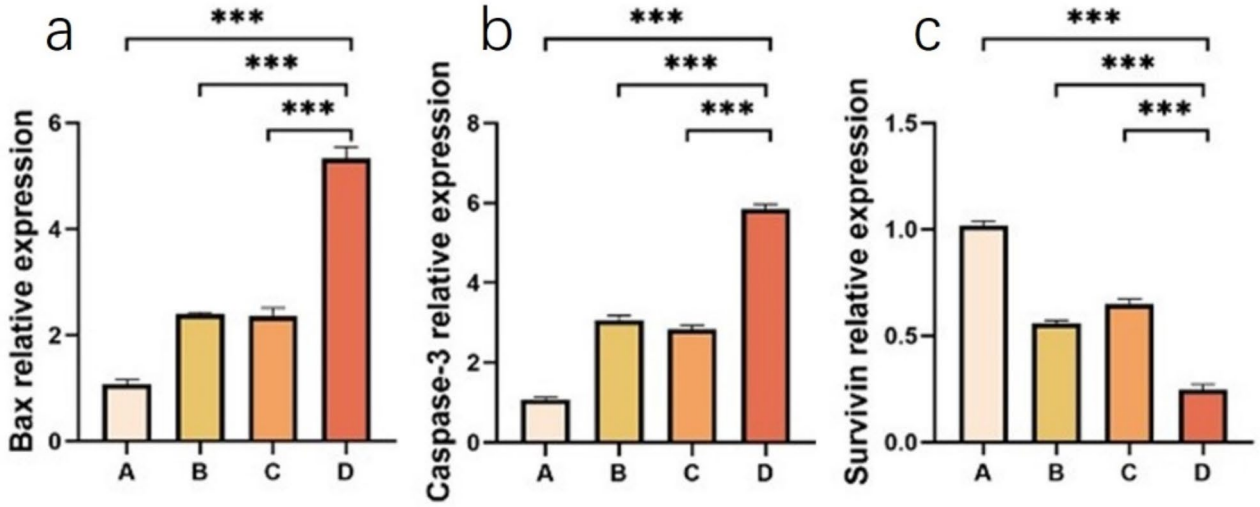

Fig. 4. Analysis of Bax, caspase-3, Survivin mRNA expression levels in transplanted tumor tissues of nude mice treated with PDT in combination with drugs. A control group, B cisplatin alone group, C PDT alone group, D cisplatin combined with PDT group. PS: ***Statistically significant difference between the cisplatin combined with PDT group compared to the other three groups, $p < 0.05$.

Detection of mRNA expression levels of Bax, caspase-3 and Survivin in transplanted tumor tissues of nude mice treated with PDT in combination with drugs

The RT-qPCR results of this experiment showed that compared with the control group, the relative expression of Bax and caspase-3 mRNA in the cisplatin alone group, the PDT alone group and the combination group were significantly increased, and the levels of Bax and caspase-3 mRNA in the combination group were higher than those in the control group, the cisplatin alone group and the PDT alone group, and the difference was statistically significant ($P < 0.05$). Survivin mRNA relative expression levels were significantly reduced, and the differences were statistically significant ($P < 0.05$). Detailed description can be found in Fig. 4.

Measurement of protein expression of Bax, caspase-3, and survivin in nude mice

The Western blot results of this experiment showed that compared with the control group, the relative protein expression of Bax and caspase-3 was significantly increased in the cisplatin alone group, the PDT alone group and the combination group, with statistically significant differences ($P < 0.05$), and the relative protein expression levels of Bax and caspase-3 in the combination group were higher than those in the cisplatin alone group and the PDT alone group, with statistically significant differences ($P < 0.05$). The relative protein expression of Survivin was significantly reduced, and the difference was statistically significant compared with the other 3 groups ($P < 0.05$), and the relative protein expression level of Survivin in the combination group was lower than that in the cisplatin alone group and the PDT alone group, with a statistically significant difference ($P < 0.05$). Detailed description can be found in Fig. 5(original blots/gels are presented in Supplementary Figure S 2.).

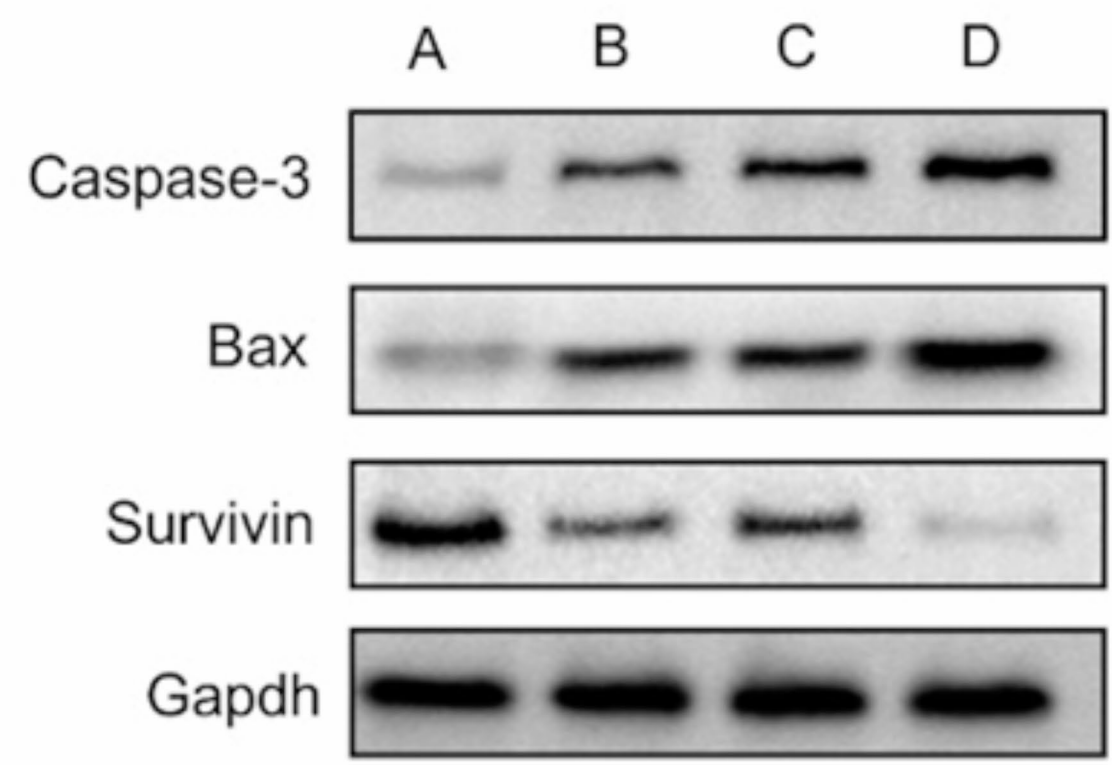

Fig. 5. Protein development results for Bax, caspase-3, and Survivin. (**A**) Control group, (**B**) cisplatin alone group, (**C**) PDT alone group, (**D**) cisplatin combined with PDT group.

Discussion

Numerous studies demonstrate that PDT can enhance respiratory function by shrinking tumors and alleviating airway blockages in patients with advanced inoperable cancer receiving palliative care[19]. In a study by Moghissi, PDT reduced endobronchial obstruction from 85.8 to 17.5% in 100 patients with advanced IIIA-IV bronchopulmonary cancer, 82% of whom had prior radiation or chemotherapy, also showing improvements in pulmonary function tests[20]. Although not as curable as early-stage lung cancer, PDT offers another treatment possibility for patients with poor pulmonary function where removal of the primary tumor would severely compromise respiratory function.

PDT's antitumor effect is well-established, with cell death mechanisms involving apoptosis, necroptosis, and macrophage-induced lysosomal degradation. Recent findings indicate that damaged tissues post-PDT release Damage-Associated Molecular Patterns (DAMPs) like calreticulin, Hsp70, and others, activating immune cells and inducing Immunogenic Cell Death (ICD). This immune response further strengthens PDT's antitumor effect[21–23].

PDT-induced apoptosis and necrosis levels depend on the intracellular reactive oxygen species (ROS) concentration after treatment[24]. However, the short half-life and limited diffusion of singlet oxygen within cells results in incomplete cell death, increasing the risk of distant cancer recurrence. Therefore, combination chemotherapy becomes even more relevant. The control of systemic disease by chemotherapeutic agents compensates for the inability of PDT to treat systemic metastases of advanced cancer. Kimura demonstrated the safety and efficacy of PDT in combination with chemotherapy in a clinical trial[25]. Hong et al. reported that systemic chemotherapy and PDT treatment may have a synergistic effect, resulting in improved survival and quality of life in patients with advanced bile duct cancer[26]. In animal studies, the combination of chemotherapy and PDT resulted in significantly larger tumor necrosis areas, higher apoptosis-positive cell percentages and increased VEGF-producing cell percentages compared to chemotherapy or PDT alone, indicating a potential synergistic effect of the combined treatment approach[27]. This may be related to the induction of oxidative stress, local inflammation, and vascular injury by PDT within the therapeutic field. These responses lead to increased expression of angiogenic factors and cytokines, resulting in decreased vascular permeability and increased deposition of chemotherapeutic agents in the tissues, leading to improved therapeutic efficacy and reduced toxicity to non-target organs[28].

Previous studies demonstrated the cell-killing effect of PDT increases with higher Hematoporphyrin Derivative (HPD) concentrations and infrared laser energy density within a specific range. By comparing the impact of various HPD concentrations and laser power densities on lung adenocarcinoma cell survival, the optimal treatment parameters for A549 cells were identified as a laser power density of 50mW/cm² and an HPD concentration of 15 μg/mL[29]. Referring to the relevant literature on animal experiments, we further adjusted the energy density to 80 mW/cm[230]. The study revealed that PDT, cisplatin, and their combination effectively inhibit

tumor growth, with the combination demonstrating a stronger ability to induce apoptosis and impede tumor progression. HE staining confirmed the successful establishment of an A549 lung adenocarcinoma animal model. TUNEL staining demonstrated increased apoptosis in both the cisplatin and PDT groups compared to the control group, with the combination therapy group exhibiting a significantly higher number of apoptotic cells than either treatment alone. The RT-PCR results showed that the relative expression levels of Bax and caspase-3 mRNA were significantly higher in the other three groups compared with the control group, and were higher in the combination group than in the individual treatment group; Compared with the control group, the expression level of Survivin mRNA was reduced in the other three groups, and the reduced level in the combination group was much lower than that in the treatment alone group. Western blot results showed that Bax and caspase-3 protein expression levels were elevated in all three groups except the control group, and were higher in the combination group than in the individual treatment group; Survivin protein expression levels were all reduced and lower than in the treatment alone group. This not only confirms that both cisplatin and PDT can direct apoptosis, but also demonstrates that the combination is more capable of increasing the intensity of apoptosis. Apoptosis is an important mechanism for photodynamic and cisplatin tumor killing. In general, there are two pathways of apoptosis - the death receptor pathway and the cellular stress pathway, both of which are closely related to the activation of caspase-3, and thus caspase-3 is a key enzyme in apoptosis[31]. Survivin is a novel apoptosis inhibitory protein family member that can inhibit the activity of caspase-3 and caspase-7, effectively blocking apoptosis triggered by various stimuli. Survivin interacts with cyclin kinases CDK4 and CDK2, obstructing apoptotic signaling pathways and inhibiting apoptosis[32]. Elevated Bax expression alters mitochondrial membrane permeability, opening transporter pores and disrupting the mitochondrial transmembrane potential, ultimately leading to irreversible apoptosis initiation[33,34]. The increased Bax and Caspase-3 expression, along with decreased Survivin levels in the combination therapy group, as compared to individual treatment groups, further validates the synergistic apoptosis-inducing effects of the combined approach. This study utilized RT-PCR and Western blot analysis to examine the effects of 630 nm laser-induced PDT, in combination with cisplatin, on Bax, Caspase-3, and Survivin expression in nude mouse xenograft tumor tissues. In conclusion, a nude mouse xenograft tumor model of human lung adenocarcinoma was established to investigate the effects and mechanisms of 630 nm laser PDT combined with cisplatin administration. Findings showed that the combination of 630 nm laser-mediated PDT and cisplatin significantly suppressed tumor growth. This may be attributed to the upregulation of Bax and Caspase-3, alongside downregulation of Survivin gene expression, ultimately promoting apoptosis and inhibiting cell proliferation. Further research is needed to explore the exact signaling pathways involved in this process.

Methods

Materials

RPMI-1640 medium, fetal bovine serum, trypsin, and dual, antibodies (100 U/ml penicillin and 0.1 mg/ml streptomycin), were purchased from Hyclone (USA); dimethyl, sulfoxide (DMSO) was a product of Sigma, (USA). The UV-visible spectra of HPD were recorded in dimethyl sulfoxide (DMSO), the solvent used for HPD preparation. The absorption peaks of HPD were observed at 405 nm (Soret band) and 630 nm (Q-band) (showing in supplementary Figure S1). Hematoxylin-eosin (HE) staining kit and TdT-mediated dUTP nick end labeling (TUNEL) apoptosis detection kit were purchased from Roche (Switzerland); RIPA lysis buffer and BCA (acid) protein assay kit were purchased from Solarbio (China); reverse transcription kit and SYBR Green quantitative PCR kit were purchased from Solarbio (China). TaKaRa (Japan); Western blotting primary and secondary antibody dilutions were purchased from BOSTER Bio (Wuhan, China); polyvinylidene difluoride (PVDF) membranes and ECL chemiluminescence kits were obtained from MILLIPORE (USA); rabbit anti-mouse Caspase-3, rabbit anti-mouse Survivin, rabbit anti-mouse Bax, hematoporphyrin derivatives (10 mM × 1 ml in dimethyl sulfoxide), were purchased from Beijing Solarbio Company (China), and were shipped in batches and stored in a refrigerator at 4 °C under dark conditions. HPD was determined using RPMI-1640 medium. The LED-IB photodynamic therapy instrument used in the experiment was made by Wuhan Yage. It can output 630 nm of red light with an output power density of 80mW/cm2 and works in continuous mode.

Cell culture

The experimental cell line was human lung adenocarcinoma A549 cell line, primary cells were obtained from ATCC, USA. A549 cells were routinely cultured in RPMI-1640 medium containing 100 U/mL of penicillin, 0.1 g/L of streptomycin mixture, and a 0.10-volume fraction of inactivated fetal bovine serum in a constant temperature incubator at 37 ℃ and 5% CO_2. When the cell viability is satisfactory by Trypan blue staining, each nude mouse is inoculated with a total of 200 µl.

Animal model construction

24 5–6 weeks-old female BALB/c nude mice, weighing 14–16 g, were obtained from Beijing Viton Lihua Laboratory Animal Technology Co. and housed in an SPF-grade animal laboratory for a week to acclimate. A cell suspension with a concentration of 1×10^7 logarithmically growing human lung adenocarcinoma A549 cells was prepared. Mice were then aseptically inoculated on the right back with 0.2 ml of the suspension. The mental state, activity, and subcutaneous tumor growth of the nude mice were observed following inoculation. Tumor size was measured every 2 days.

When the average tumor volume reached 100–150 mm^3, it could be used for experiments. 24 tumor-bearing nude mice were randomly divided into 4 groups: control group (no chemotherapeutic drug and PDT), cisplatin alone group (chemotherapeutic drug but no PDT), PDT alone group (PDT only, but no chemotherapeutic drug), and combination group (administration of chemotherapeutic drug followed by PDT). Control group: saline was injected intraperitoneally in nude mice at a dose of 5 mg/kg. Cisplatin alone group: cisplatin was

injected intraperitoneally in nude mice at a dose of 5 mg/kg for a total of 1 time. PDT alone group: multiple exposures were used at low doses. That is, the photosensitizer was injected into the tumor at a dose of 10 mg/kg. After 48 h of light avoidance, each nude mouse was anesthetized using isoflurane inhalation, and after that, it was irradiated with a 630 nm laser with an energy density of 80 mW/cm^2 for 10 min at a distance of 5 cm. For PDT treatment, only the tumors of the nude mice were exposed, and the rest of the tumor was covered with a black cloth in order to prevent irradiation of the normal skin of the nude mice. Irradiation was performed every 2 days for a total of 3 times. Cisplatin combined with PDT group: first intraperitoneal injection of cisplatin followed by PDT treatment. In this study, cisplatin and the photosensitizer (HPD) were not chemically combined but were administered sequentially as part of the combination therapy. Tumor specimens from all 4 groups were taken 3 days after the last irradiation(Fig. 6). One part was placed in 4% paraformaldehyde solution for 24 h for HE and TUNEL staining, and the other part was stored in a refrigerator at -80 °C for real-time PCR and Western blot. The mice were killed by carbon dioxide asphyxiation. The experiment was conducted in strict compliance with animal ethics.

HE staining

Fresh tissue (thickness not exceeding 0.5 cm) was taken, washed with saline, placed in 4% paraformaldehyde fixative, and removed after 24 h of fixation. Water was gradually removed from the tissues with low to high concentrations of ethanol, and the dehydrated tissues were transparent in xylene, which was used to replace the ethanol in the tissues to show varying degrees of transparency. The clear tissue was then embedded by placing it in dissolved paraffin melt and completely immersing the paraffin into the tissue block. The embedded tissue block solidified and hardened, then the wax block was fixed on a slicer to cut into 5 to 8 μm slices, and finally attached to slides to dry. Before staining, paraffin was removed from the sections with xylene, then rehydrated with high to low concentrations of ethanol, and finally washed with distilled water for staining. The stained sections were dehydrated with ethanol, transparent with xylene and then closed, and the changes in tissue morphology and structure were observed under a light microscope.

TUNEL apoptosis assay

Follow the steps described in the TUNEL Apoptosis Detection Kit to observe apoptosis under a microscope. Apoptotic cells were standardized as nuclei consolidated or fragmented, chromosomes fragmented or aggregated, and nuclei brown or tan in color. Apoptosis-positive cells were counted in five random fields under high magnification and were considered positive by the presence of brown granules in the nucleus. Apoptosis rate = number of apoptotic cells/total number of cells observed × 100%.

Real-time fluorescence quantitative PCR (RT-PCR)

Total RNA was extracted from cells using TaKaRa reagent according to the manufacturer's instructions, and its concentration was measured with a microplate reader. Single-stranded cDNA was synthesized by reverse transcription with oligo(dT) primers. RT-PCR was performed with the following cycling conditions: initial activation at 95 °C for 10 min, followed by 40 cycles of denaturation at 95 °C for 5 s, annealing at 60 °C for 30 s, and extension at 60 °C for 3 min. Ct values were recorded for each group, and relative gene expression levels ($2^{-\Delta\Delta Ct}$) were calculated using β-actin as an internal reference. Primers are listed in Table 2.

Statistical analysis

SPSS23.0 statistical software was used for statistical analysis. Each group of experiments was independently repeated three times, and the experimental data were expressed as mean ± standard deviation (x ± s). A one-way

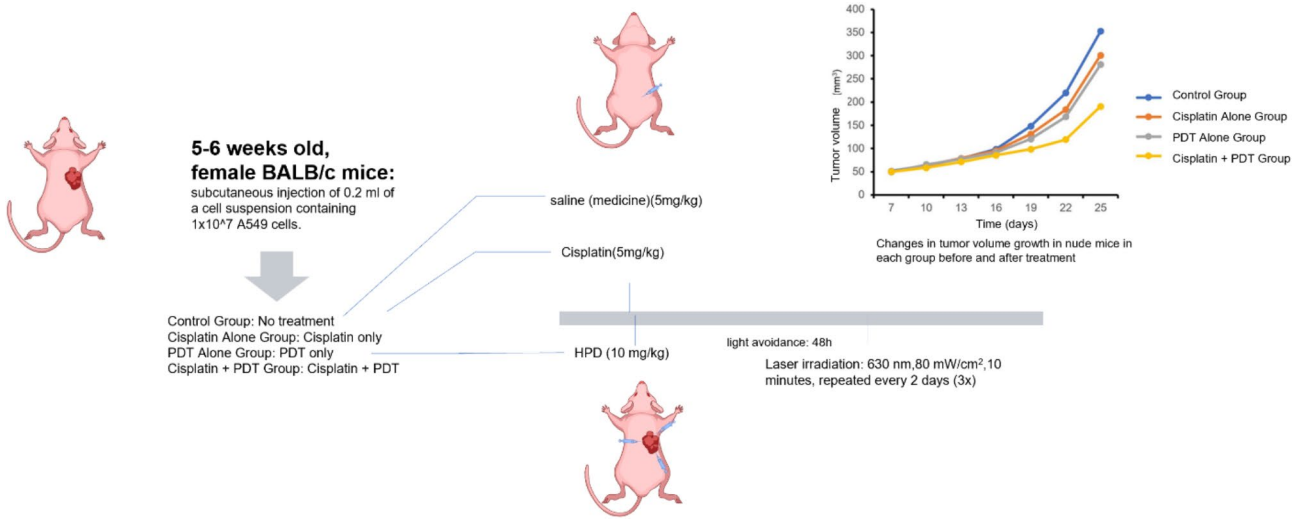

Fig. 6. schematic illustration.

Gene	Primer sequences (5′–3′)	
	Pre-primers	Post-primers
Bax	AGCGACTGATGTCCCTGTCT	CTCAGCCCATCTTCTTCCAG
Survivin	GCCCAGTGTTTCTTCTGCTT	TCTCCGCAGTTTCCTCAAAT
caspase-3	GTGGAGGCCGACTTCTTGTA	TGTCGGCATACTGTTTCAGC
β-actin	TGGCACCCAGCACAATGAA	CTAAGTCATAGTCCGCCTAGAAGCA

Table 2. PCR primer sequences.

ANOVA was used to analyze the difference between multiple groups. Pairwise comparisons between groups were analyzed using the LSD-t test. $p \leq 0.05$ indicated that the differences were statistically significant.

Data availability

Data is provided within the manuscript.The datasets analyzed during the current study are available in the GEO repository, https://www.ncbi.nlm.nih.gov/nuccore/NM_001291428.2, https://www.ncbi.nlm.nih.gov/nuccore/NM_001354777.2.

Received: 5 December 2024; Accepted: 18 March 2025
Published online: 24 March 2025

References

1. Thai, A. A., Solomon, B. J., Sequist, L. V., Gainor, J. F. & Heist, R. S. Lung cancer. *Lancet* **398**, 535–554 (2021).
2. Pope, C. A. et al. Lung cancer and cardiovascular disease mortality associated with ambient air pollution and cigarette smoke: Shape of the exposure-response relationships. *Environ. Health Perspect.* **119**, 1616–1621 (2011).
3. Mutsaers, A. et al. Uncovering the armpit of SBRT: An institutional experience with stereotactic radiation of axillary metastases. *Clin. Transl Radiat. Oncol.* **45**, 100730 (2024).
4. Wilson, B. C. & Patterson, M. S. The physics, biophysics and technology of photodynamic therapy. *Phys. Med. Biol.* **53**, R61–109 (2008).
5. Reginato, E., Wolf, P. & Hamblin, M. R. Immune response after photodynamic therapy increases anti-cancer and anti-bacterial effects. *World J. Immunol.* **4**, 1–11 (2014).
6. Bhattacharya, D. et al. Recent developments in photodynamic therapy and its application against multidrug resistant cancers. *Biomed. Mater.* **18**, 062005 (2023).
7. Rigual, N. et al. Photodynamic therapy with 3-(1'-hexyloxyethyl) pyropheophorbide a for cancer of the oral cavity. *Clin. Cancer Res.* **19**, 6605–6613 (2013).
8. You, D. G. et al. ROS-generating TiO_2 nanoparticles for non-invasive sonodynamic therapy of cancer. *Sci. Rep.* **6**, 23200 (2016).
9. Canti, G., De Simone, A. & Korbelik, M. Photodynamic therapy and the immune system in experimental oncology. *Photochem. Photobiol Sci.* **1**, 79–80 (2002).
10. Wachowska, M., Muchowicz, A. & Demkow, U. Immunological aspects of antitumor photodynamic therapy outcome. *Cent. Eur. J. Immunol.* **40**, 481–485 (2015).
11. Anzengruber, F., Avci, P., de Freitas, L. F. & Hamblin, M. R. T-cell mediated anti-tumor immunity after photodynamic therapy: why does it not always work and how can we improve it? *Photochem. Photobiol. Sci.* **14**, 1492–1509 (2015).
12. Pantiushenko, I. V. et al. Development of bacteriochlorophyll a-based near-infrared photosensitizers conjugated to gold nanoparticles for photodynamic therapy of cancer. *Biochemistry (Mosc).* **80**, 752–762 (2015).
13. Vrouenraets, M. B. et al. Targeting of aluminum (III) phthalocyanine tetrasulfonate by use of internalizing monoclonal antibodies: improved efficacy in photodynamic therapy. *Cancer Res.* **61**, 1970–1975 (2001).
14. Carcenac, M. et al. Internalisation enhances photo-induced cytotoxicity of monoclonal antibody-phthalocyanine conjugates. *Br. J. Cancer.* **85**, 1787–1793 (2001).
15. Faber, M., Coudray, C., Hida, H., Mousseau, M. & Favier, A. Lipid peroxidation products, and vitamin and trace element status in patients with cancer before and after chemotherapy, including Adriamycin. A preliminary study. *Biol. Trace Elem. Res.* **47**, 117–123 (1995).
16. Morabito, A. et al. Trastuzumab in combination with gemcitabine and Vinorelbine as second-line therapy for HER-2/neu overexpressing metastatic breast cancer. *Oncol. Rep.* **16**, 393–398 (2006).
17. Oliveira, C. et al. Immune-related serious adverse events with immune checkpoint inhibitors: Systematic review and network meta-analysis. *Eur. J. Clin. Pharmacol.* **80**, 677–684 (2024).
18. Rossi, C. R. et al. Pharmacokinetics of intraperitoneal cisplatin and doxorubicin. *Surg. Oncol. Clin. N. Am.* **12**, 781–794 (2003).
19. Dougherty, T. J. et al. Photodynamic therapy. *J. Natl. Cancer Inst.* **90**, 889–905 (1998).
20. Moghissi, K. et al. The place of bronchoscopic photodynamic therapy in advanced unresectable lung cancer: experience of 100 cases. *Eur. J. Cardiothorac. Surg.* **15**, 1–6 (1999).
21. Kiesslich, T., Krammer, B. & Plaetzer, K. Cellular mechanisms and prospective applications of hypericin in photodynamic therapy. *Curr. Med. Chem.* **13**, 2189–2204 (2006).
22. Garg, A. D. et al. Immunogenic cell death, damps and anticancer therapeutics: An emerging amalgamation. *Biochim. Biophys. Acta.* **1805**, 53–71 (2010).
23. Yang, J. K., Kwon, H. & Kim, S. Recent advances in light-triggered cancer immunotherapy. *J. Mater. Chem. B.* **12**, 2650–2669 (2024).
24. Dysart, J. S. & Patterson, M. S. Characterization of Photofrin photobleaching for singlet oxygen dose estimation during photodynamic therapy of MLL cells in vitro. *Phys. Med. Biol.* **50**, 2597–2616 (2005).
25. Kimura, M., Miyajima, K., Kojika, M., Kono, T. & Kato, H. Photodynamic therapy (PDT) with chemotherapy for advanced lung cancer with airway stenosis. *Int. J. Mol. Sci.* **16**, 25466–25475 (2015).
26. Hong, M. J., Cheon, Y. K., Lee, E. J., Lee, T. Y. & Shim, C. S. Long-term outcome of photodynamic therapy with systemic chemotherapy compared to photodynamic therapy alone in patients with advanced hilar cholangiocarcinoma. *Gut Liver.* **8**, 318–323 (2014).
27. Nonaka, Y. et al. Synergic effect of photodynamic therapy using talaporfin sodium with conventional anticancer chemotherapy for the treatment of bile duct carcinoma. *J. Surg. Res.* **181**, 234–241 (2013).

28. Kim, S. C., Rho, M. C., Lee, H. S., Kim, Y. K. & Kim, K. Caspase-3-dependent apoptosis in vascular smooth muscle cell by proteasome Inhibition. *J. Cardiovasc. Pharmacol.* **42**, 554–560 (2003).
29. Martinou, J. C. & Youle, R. J. Mitochondria in apoptosis: Bcl-2 family members and mitochondrial dynamics. *Dev. Cell.* **21**, 92–101 (2011).
30. Shafirstein, G. et al. In vivo models for studying interstitial photodynamic therapy of locally advanced cancer. *Methods Mol. Biol.* **2451**, 151–162 (2022).
31. Rogers, C. et al. Cleavage of DFNA5 by caspase-3 during apoptosis mediates progression to secondary necrotic/pyroptotic cell death. *Nat. Commun.* **8**, 14128 (2017).
32. Wolf, P., Schoeniger, A. & Edlich, F. Pro-apoptotic complexes of BAX and BAK on the outer mitochondrial membrane. *Biochim. Biophys. Acta Mol. Cell. Res.* **1869**, 119317 (2022).
33. Tsujimoto, Y. Role of bcl-2 family proteins in apoptosis: Apoptosomes or mitochondria? *Genes Cells.* **3**, 697–707 (1998).
34. Yang, J., Liu, F. X. & Yan, X. C. [research advances on inhibitor of apoptosis, survivin]. *Ai Zheng.* **22**, 771–774 (2003).

Author contributions
C.Lin. and T.Li. conceived the experiment, T.Li. and L.Li. conducted the experiment, M.Shao, Y.Dong. and X.Yang. analyzed the results. All authors reviewed the manuscript.

Declarations

Competing interests
The authors declare no competing interests.

Ethics approval
This study is approved by Ethics Committee of The Animal Care & Welfare Committee of The Affiliated Hospital of Qingdao University (No. AHQU-MAL20200911). All procedures were conducted in full compliance with the ARRIVE guidelines. For the accordance statement, all methods were carried out in accordance with relevant guidelines and regulations.

Additional information
Supplementary Information The online version contains supplementary material available at https://doi.org/10.1038/s41598-025-94990-3.

Correspondence and requests for materials should be addressed to C.-z.L.

Reprints and permissions information is available at www.nature.com/reprints.

Publisher's note Springer Nature remains neutral with regard to jurisdictional claims in published maps and institutional affiliations.